Three-Dimensional Velocity Obstacle Method for Uncoordinated Avoidance Maneuvers of Unmanned Aerial Vehicles

Jenie, Yazdi; van Kampen, EJ; de Visser, CC; Ellerbroek, J; Hoekstra, JM

DOI
10.2514/1.G001715

Publication date
2016

Document Version
Accepted author manuscript

Published in
Journal of Guidance, Control, and Dynamics: devoted to the technology of dynamics and control

Citation (APA)
Jenie, Y., van Kampen, EJ., de Visser, CC., Ellerbroek, J., & Hoekstra, JM. (2016). Three-Dimensional Velocity Obstacle Method for Uncoordinated Avoidance Maneuvers of Unmanned Aerial Vehicles. *Journal of Guidance, Control, and Dynamics: devoted to the technology of dynamics and control*, *39*(10), 2312-2323. https://doi.org/10.2514/1.G001715

Three-Dimensional Velocity Obstacle Method for Uncoordinated Avoidance Maneuvers of Unmanned Aerial Vehicles

Yazdi I. Jenie* Erik-Jan van Kampen† Cornelis C. de Visser‡ Joost Ellerbroek§ Jacco M. Hoekstra¶

Control and Simulation Section, Faculty of Aerospace Engineering, Delft University of Technology

This paper proposes a novel avoidance method called the Three-Dimensional Velocity Obstacle (3DVO) method. The method is designed for Unmanned Aerial Vehicle (UAV) applications, in particular to autonomously handle uncoordinated multiple encounters in an integrated airspace, by exploiting the limited space in a three-dimensional manner. The method is a three-dimensional extension of the Velocity Obstacle method that can reactively generate an avoidance maneuver by changing the vehicle velocity vector based on the encounter geometry. Adverse maneuvers of the obstacle are anticipated by introducing the concept of a buffer velocity set, which ensures that the ownship will diverge with sufficient space in case of sudden imminence. A three-dimensional resolution is generated by choosing the right plane for avoidance, in which the UAV conducts a pure turning maneuver. Implementation of the 3DVO method is tested in several simulations that demonstrate its capability to resolve various three-dimensional conflicts. A validation using Monte Carlo simulations is also conducted in stressful super-conflict scenarios, which results in zero collisions occurrences for the entire 25,000 samples.

Nomenclature

BV	Buffer Velocity set
CC	Collision Cone set
$\mathbf{P}_\phi$	Avoidance Plane at the angle ϕ
$\mathbf{RV_i}$	Obstacle Reachable Velocity set
$\mathbf{S_{pz}}$	Protected Zone
$\mathbf{VO_{P_\phi}}$	Velocity Obstacle section on Avoidance Plane-ϕ
VO	Velocity Obstacle set
α_{vo}	Opening angle of the Velocity Obstacle Cone, [-]
Δt	Time-step of the **VO** set generation, [s]
$\delta_{\mathbf{P}}$	Dihedral angle of the avoidance-plane from the XY-plane, [-]
$\omega_{a.cr}$	Critical avoidance turning rate, [-/s]
ω_{avo}	Avoidance turning rate, [-/s]
$\phi_{\mathbf{P}}$	Angle of Avoidance Plane around X-axis
ψ_{oi}	Azimuth angle of the obstacle-i from the ownship, [-]
σ_{col}	Standard Distribution of Collision Probability, [-]
θ_{oi}	Elevation angle of the obstacle-i from the ownship, [-]
$\vec{A}_{vo}$	Apex position of the Velocity Obstacle cone, [m]
$\vec{D}_{vo}$	Velocity Obstacle cone symmetric axis vector, [m]
$\vec{E}^{\phi}_{vo}$	Escaping point of a **VO** set, [m/s]

*PhD Student, Faculty of Aerospace Engineering, Delft University of Technology, 2629HS, Delft, The Netherlands
†Assistant Professor, Faculty of Aerospace Engineering, Delft University of Technology, 2629HS, Delft, The Netherlands
‡Assistant Professor, Faculty of Aerospace Engineering, Delft University of Technology, 2629HS, Delft, The Netherlands
§Assistant Professor, Faculty of Aerospace Engineering, Delft University of Technology, 2629HS, Delft, The Netherlands
¶Professor, Faculty of Aerospace Engineering, Delft University of Technology, 2629HS, Delft, The Netherlands

$\vec{V}_i$	Obstacle velocity vector, [m/s]
$\vec{V}_o$	Ownship velocity vector, [m/s]
$\vec{V}_R$	Relative velocity between the ownship and the obstacle, [m/s]
$\vec{V}_{avo}^{\phi}$	Avoiding velocity vector on Avoiding Plane $\mathbf{P}_\phi$, [m/s]
$\vec{X}_i$	Obstacle position relative to the ownship, [m]
$\vec{X}_o$	Ownship position, [m]
d_{avo}	Avoidance starting distance, [m]
d_{oi}	Distance between the ownship and the obstacle-i, [m]
d_{vo}	Length of the Velocity Obstacle cone, [m]
N_{col}	Total Collision Occurrence for N_{MC}, [-]
n_{col}	Collision Occurrence of a Case Sample, [-]
N_{MC}	Number of Monte-Carlo simulation samples, [-]
P_{col}	Collision Probability, [-]
r_{pz}	Radius of the Protected Zone, [m]
r_{rvi}	Radius of the obstacle Reachable Velocity set, [m]
r_{vo}	Radius of the effective base of the Velocity Obstacle cone, [m]

I. Introduction

For Unmanned Aerial Vehicles (UAV) to be integrated into the airspace system, they are required to have an autonomous Conflict Detection and Resolution (CD&R) system that can demonstrate an adequate level of safety during its operation.[1] In this context, a UAV will encounter dynamic obstacles, such as manned aircraft and other UAVs, that can be negligent in avoidance, move in an unpredictable way, or actually seek a collision (hostile). These kinds of situations can only be detected independently by relying on sensors on-board, since the counterparts do not cooperatively broadcast their flight data and intention. As a result, the space for avoidance will be limited by the sensor range of detection. The resolution maneuver, therefore, needs to fully exploit the remaining space left, while anticipating the possible movement of those counterparts. To be able to reach safety as fast as possible, a resolution maneuver has to be aggressively conducted with the maximum performance of the UAV, comprehend several obstacles in the traffic at once, and neglect any original mission or trajectory. Ref.2 describes this type of avoidance situation and resolution as an Escape CD&R approach.

Reactive collision-avoidance methods are potentially the most suitable to support an escape maneuver autonomously. These methods rely on the instantaneous situation detection to quickly calculate the avoidance maneuver, instead of depending on predetermined data or extensive iteration that might be optimized, but processed slower, such as in Local Path Planning methods[3,4] or Dynamic Programming.[5] Several reactive avoidance methods can be found in the literature, including the Potential Field method,[6–9] and Geometric guidance methods such as the Collision Cone[10,11] or the Velocity Obstacle method.[12–23] Since they are less computationally intensive, these reactive methods are promising in providing a fast avoidance solution in a dynamic environment.

Most of those methods, however, include several simplifying assumptions that limit their practical use for an escape situation. Those assumptions include one or more of the following: generates resolutions only in two-dimensional space, involves only homogeneous vehicles, non-maneuvering obstacles, and only for a coordinated avoidance. The methods demonstrated in 11 and 24 are among the few that provide both encounter handling and resolution generation in three dimensions which are able to significantly expand the resolutions in a limited avoidance space. Those methods, however, are demonstrated only in handling static or non-maneuvering obstacles. The work of 14, 19, and 21 are examples that consider maneuvering obstacles, but in a homogeneous coordinated situation where the vehicles have uniform speeds and avoidance tendencies. The work of 12 presents a Selective Velocity Obstacle method that handles heterogeneous encounters, including the random maneuvers of obstacles, but the resolution is based on implicit coordination.

This paper contributes to the literature by proposing a novel reactive avoidance method called the Three-Dimensional Velocity Obstacle (3DVO) method. The method is designed to handle uncoordinated multiple encounters by exploiting the limited space as much as possible, in a three-dimensional manner. This concept is a continuation of the work originally reported in 25 by the same authors, presented here with a simpler but more complete formalization. Additional contribution of this current paper is the incorporation of the heterogeneous situation, which is evaluated in a simulation by randomizing initial speeds and turning-rates,

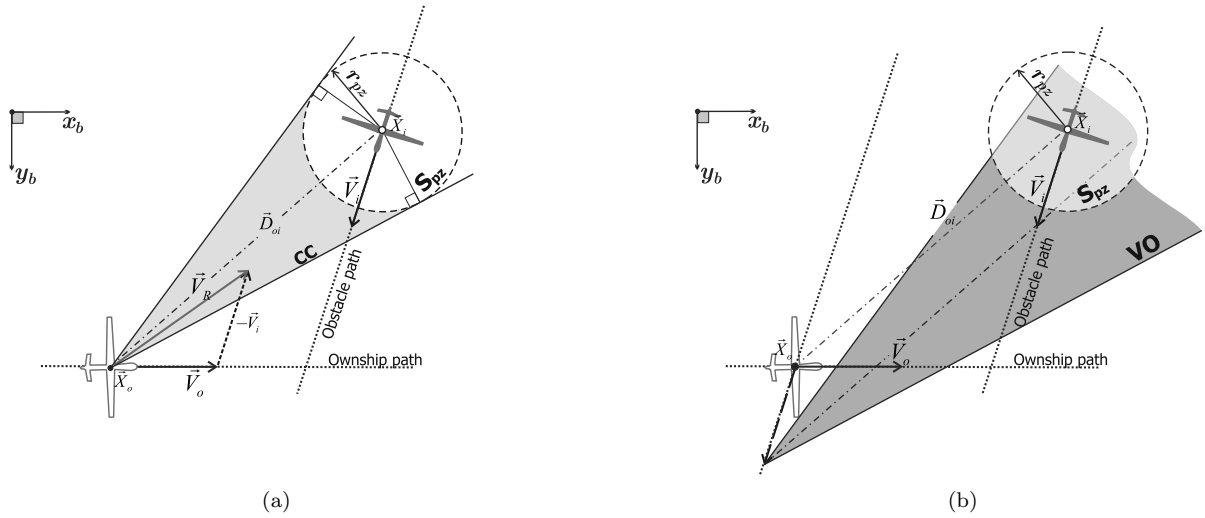

Figure 1. Graphical presentation of (a) Collision Cone and (b) The Velocity Obstacle set

to truly represent an escape situation.[2] The foundation of the 3DVO method is the Velocity Obstacle method[10,13] (VO-method), which is selected due to several advantages it has compared to other reactive methods. For instance, compared to the Potential Field method (PF-method), the VO-method was originally designed for avoiding moving obstacles by taking into account the velocity of each obstacle. The VO-method also gives a set of possible resolutions that is less prone to problems with local minimums in multiple encounter situations. Lastly, the VO-method has a more geometrically understandable appearance, which make its three-dimensional extension straightforward while keeping all its criteria and strategies.

This paper is structured as follows. Section II discusses the concept of the 3DVO method by introducing the extension of the method into three-dimensions setup. The approaches to handle maneuvering obstacles are elaborated as well, along with the introduction of the Avoidance Planes concept. After that, Section III explains possible strategies for the 3DVO method, which include the avoidance algorithm, the decision process in choosing the Avoidance Plane, and the derivation of the avoidance turning rate. Section IV presents the implementation of the three-dimensional VO-method in several simulations, where the performance of the method is demonstrated. A validation process using Monte Carlo simulation is also conducted and presented in this section. Section V ends the paper with several concluding remarks.

II. The Three-dimensional Velocity Obstacle Method

The Three-dimensional Velocity Obstacle (3DVO) method extends the use of the original VO-method,[12,13] which is applied in a two-dimensional encounter, such as shown in Figure 1-a. In every encounter case, a collision cone set (**CC**) can be drawn, which collects all relative velocity vectors between the vehicles that intersect the protected-zone ($\mathbf{S_{pz}}$): a threshold area around the obstacle. In cases of avoiding collision at a short distance, the value of $\mathbf{S_{pz}}$ radius, r_{pz} is typically the summation of the vehicles effective semi-spans. Whether the two vehicles are bound to collide or not, therefore, can be determined by the inclusion of their relative velocity $\vec{V}_R$ to the **CC**. Hence to avoid collision, the ownship needs to ensure its velocity exclusion from the **CC** set.

The VO-method uses the inclusion of the ownship absolute velocity vector $\vec{V}_o$ into the so-called Velocity Obstacle set (**VO**), which is the translation of **CC** along the velocity of the obstacle, $\vec{V}_i$, as shown in Figure 1-b. To avoid the obstacle, the ownship needs to change its velocity vector to a point outside the **VO**.

The VO-method extension into the 3DVO method includes the detection of three-dimensional conflicts, and the generation of possible avoiding routes that also exploit the three-dimensional space around the ownship. This section explains the detection part by converting the sets of the VO-method to a three-dimensional definition. The algorithm to reactively generate the avoiding routes, along with the strategy for avoidance, is explained in Section III.

A. 3DVO method's Velocity Obstacle Cone

The concept of the VO-method is extended for three-dimensional cases by first redefining the protected zone, $\mathbf{S_{pz}}$, from a circle to a three-dimensional form. There are two types of $\mathbf{S_{pz}}$ commonly found in the literature, either spherical,[25,26] or cylindrical.[20,21,24] This paper uses the spherical protected-zone definition that can represent general UAV encounters and resolutions better than a cylindrical in the three-dimensional space. The reason is that unlike manned aircraft, a UAV, especially of rotary-wing type, can have a much more flexible trajectory in any direction by exploiting the entire space around it, and hence it needs to consider collisions from any three-dimensional direction. A spherical protected zone in this case will treat encountering obstacles equally regardless of the direction and orientation.

Consider a three-dimensional encounter case between an avoiding vehicle (or an ownship) and an obstacle, as depicted in figure 2. Similar to the two-dimensional case, the Collision Cone **CC** can be derived by collecting every relative velocity $\vec{V}_R$ whose positive elongation intersects the $\mathbf{S_{pz}}$ sphere. In this three-dimensional case, the **CC** takes the shape of an infinite right-cone with size and orientation corresponding to the dimension of $\mathbf{S_{pz}}$ and the obstacle position $\vec{X}_i$, relative to the ownship. The apex of **CC** is the ownship position $\vec{X}_o$, where every tangential line from $\vec{X}_o$ to the edge of $\mathbf{S_{pz}}$ is a generating line of the cone (generatrix).

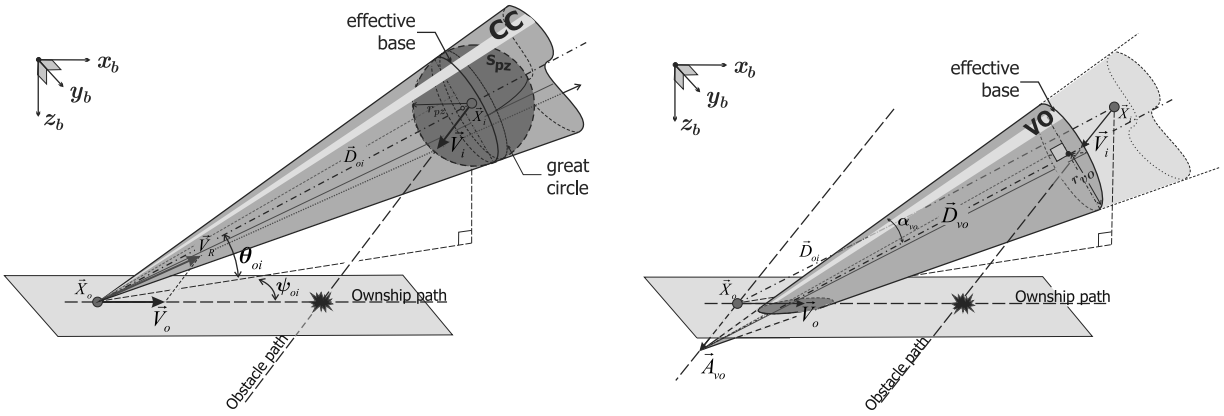

(a) (b)

Figure 2. Three-dimensional velocity obstacle set definition. (a) the Collision Cone CC, (b) Translated CC cone to the Velocity Obstacle set VO

Similar to the two-dimensional case, the Velocity Obstacle set is obtained by translating the **CC** cone in three-dimensions along $\vec{V}_i$ from $\vec{X}_o$, as shown in Figure 2-b. With this set, the collision criterion between two vehicles in three-dimensional space can be defined: an ownship will eventually collide if and only if its velocity vector $\vec{V}_o$ is included in the corresponding **VO** cone, i.e., $\vec{V}_o \in \mathbf{VO}$.

The three-dimensional **VO** can be defined using a cross-section perpendicular to the cone axis as an effective base. This paper uses the cross-section that is rimmed by the $\mathbf{S_{pz}}$ intersection with the cone, as shown in Figure 2-a. Thus, the **VO** cone is defined by three parameters: the position of its apex, $\vec{A}_{vo}$, the length and orientation of the axis, $\vec{D}_{vo}$, and the radius of the effective base, r_{vo}. These parameters are mathematically expressed in equations (1) and (2) as functions of $\mathbf{S_{pz}}$ radius and the obstacle position in spherical coordinates (distance d_{oi}, elevation θ_{oi}, and azimuth ψ_{oi}) with respect to the ownship frame of reference ($\vec{X}_o$ as the origin). The cone opening angle, α_{vo}, is also defined in equation (1). Note that the effective base of the cone does not coincide with the great-circle of $\mathbf{S_{pz}}$, as depicted in Figure 2-a.

$$d_{vo} = \frac{d_{oi}^2 - r_{pz}^2}{d_{oi}}, \qquad r_{vo} = r_{pz}\frac{\sqrt{d_{oi}^2 - r_{pz}^2}}{d_{oi}}, \qquad \alpha_{vo} = \arctan\left(\frac{r_{vo}}{d_{vo}}\right) \tag{1}$$

$$\vec{A}_{vo} = \vec{V}_i, \qquad \text{and} \quad \vec{D}_{vo} = \begin{bmatrix} \cos\theta_{oi}\cos\psi_{oi} \\ \cos\theta_{oi}\sin\psi_{oi} \\ \sin\theta_{oi} \end{bmatrix} d_{vo}. \tag{2}$$

The inclusion of the $\vec{V}_o$ vector end point in the **VO** cone can be determined by checking the angle between the vector from the cone apex, $\vec{A}_{vo}$, and the cone axis. Equation (3) represents the criteria of inclusion using the vector inner product. The second term in equation (3) is to ensure the imminence of the encounter by the avoidance starting point, d_{avo}, since the first criterion is unbounded, representing the possible collision within infinite time in the future. Thus,

$$\vec{V}_o \in \mathbf{VO}_i \iff \left\{ \frac{\left[\vec{V}_o - \vec{A}_{vo}\right] \cdot \vec{D}_{vo}}{\left|\vec{V}_o - \vec{A}_{vo}\right| d_{vo}} > \cos\alpha_{vo} \quad \text{and} \quad d_{oi} < d_{avo} \right\}. \tag{3}$$

The **VO** cone expands as the two vehicles converge, and shrinks as they diverge. When the α_{vo} reaches $\pi/2$, the ownship position is exactly on the surface of the protected zone $\mathbf{S_{pz}}$, or $d_{oi} = r_{pz}$, as indicated in equation (1). A degenerate case happens when the two vehicles collide, or when $d_{oi} < r_{pz}$, in which case the **VO** cone cannot be defined.

Finally, multiple encounters are accommodated in the three-dimensional setup by taking the summation of the **VO** sets. Let $i = 1, 2, 3, ..., N$ be the indexes of N-imminent obstacles under consideration, then the overall **VO** for a multiple encounter case is the union of the Velocity Obstacle set, or $\bigcup_i \mathbf{VO}_i$. The ownship velocity vector is included in the overall set if it is included in at least one of the $\mathbf{VO_i}$ or

$$\vec{V}_o \in \bigcup_i \mathbf{VO}_i \iff \exists i : \vec{V}_o \in \mathbf{VO}_i. \tag{4}$$

B. Handling Maneuvering Obstacles: The Buffer Velocity Set

The challenges in using the VO-method in situations where the obstacles are maneuvering have been addressed in previous studies. The work of 15 describes the problem of oscillation and the reciprocal dance in cases of two-dimensional conflicts, where each of the vehicles attempts avoidance using the VO-method. These problems, which can cause a failed avoidance, are commonly solved using an implicit coordination of avoidance.[12,19,21] However, in an uncoordinated situation the problems reappear with an additional problem of a sudden imminence. This last problem occurs when a vehicle adversely changes its course in close proximity to another, such that there is no sufficient space or time left to conduct the sudden avoidance.

An extra set can be added to the Velocity Obstacle set in order to handle the possible maneuver of an obstacle. Consider the case shown in Figure 3-a. Within a certain time step, the ownship generates a **VO** set based on the instantaneous encounter geometry, and generates a resolution to avoid any corresponding conflicts. The time-step between two **VO** generations, denoted Δt, is assumed to be constant and represents the detection frequency of the CD&R system. During this Δt, however, the obstacle might have updated its velocity vector, such as, for instance, by a rotational maneuver within the range of $\vec{V}_i'$ to $\vec{V}_i''$. As shown in Figure 3-a, for each point on the arcs of $\vec{V}_i$, a new **VO** set can be defined, some of which might rule out the initially assumed safe zones.

If all possible maneuvers of the obstacle within the generation time Δt can be predicted, then they can be anticipated by summing all the possible **VO** sets into one big set. Figure 3-a shows this summation as a new triangle that originates at point $A^*_{vo^+}$, collecting all possible **VO** sets. The resulting triangular set, however, is not aligned with the axis of the original **VO**, and adds an extra degree of freedom for the combined **VO** definition, especially in three-dimensional cases.

Figure 3-b defines a simpler definition for the sums of **VO**s by using a circular reachable velocity set of the obstacle, $\mathbf{RV_i}$. This set collects every possible arc of $\vec{V}_i$ within Δt, from any arbitrary bearing angle between vehicles separated by a particular distance. The resulting sum of **VO** can be defined by moving the apex in the opposite direction of the $\vec{D}_{vo}$ until the entire $\mathbf{RV_i}$ is included. This definition also holds in the three-dimensional setup, where the $\mathbf{RV_i}$ is represented as a sphere as shown in the Figure 3-c. This paper denotes the extra layer of the **VO** as the Buffer Velocity set (**BV**). The combined resulting **VO**, denoted as the $\mathbf{VO}^+$, effectively takes into account the obstacle maneuver within the time-step of its generation, Δt.

The VO parameters in three dimensions are therefore redefined, as expressed in equation (5) and (6), i.e.,

$$\alpha_{vo^+} = \alpha_{vo}, \qquad \vec{A}_{vo^+} = \vec{A}_{vo} - r_{rvi}\frac{\vec{D}_{vo}}{d_{vo}\sin\alpha_{vo^+}}. \tag{5}$$

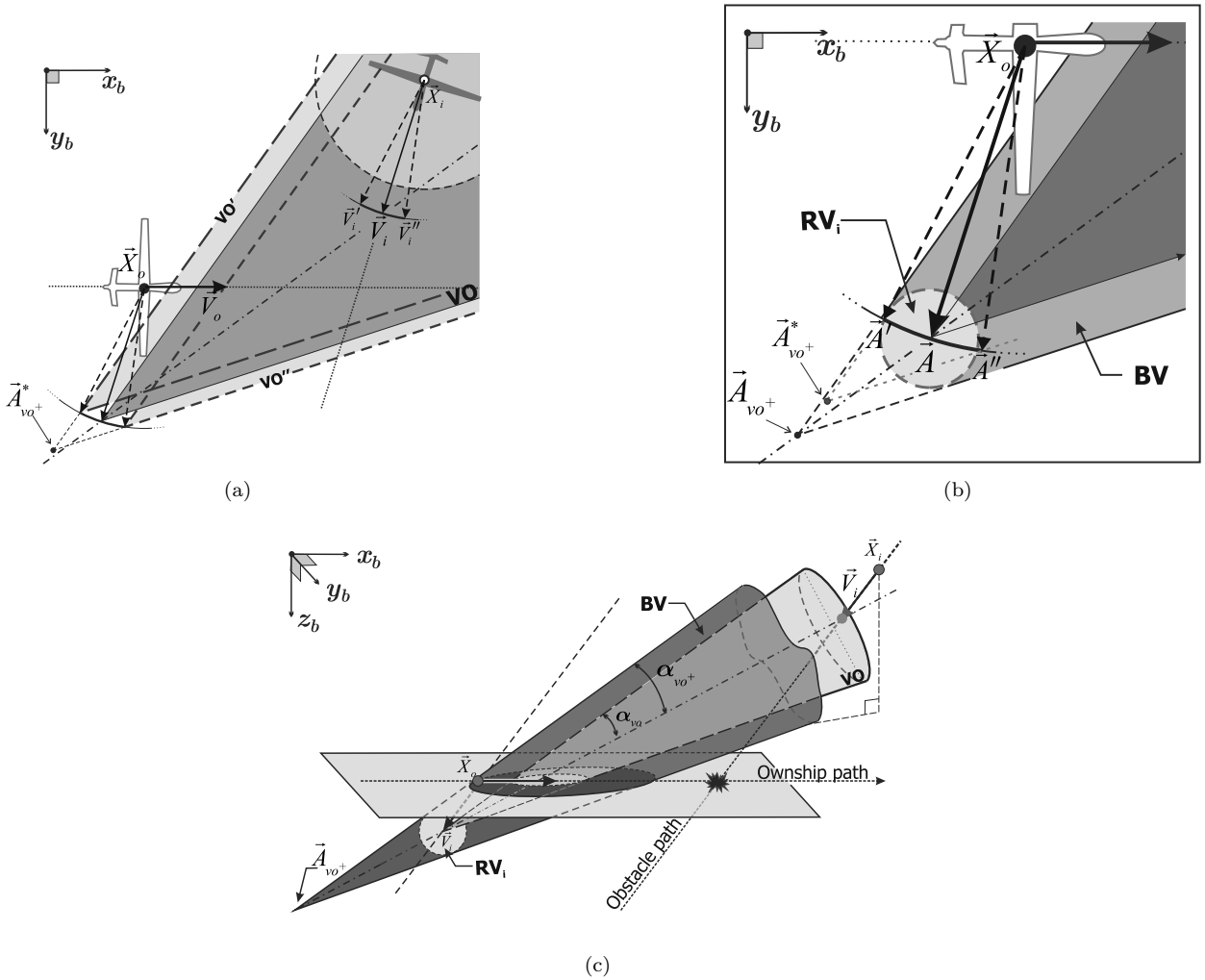

(a) (b) (c)

Figure 3. The Buffer Velocity set definition. (a) The VO sets from points in the 'arc' of possible obstacle velocities, (b) the circle of RV_i and the resulting $\mathbf{VO}^+$, in two dimensions and (c) in three dimensions

The radius of the $\mathbf{RV_i}$, r_{rvi}, depends on the assumed value of the change of heading of expected obstacles relative to the ownship, within the generation time-step, $\omega_i \Delta t$. The radius r_{rvi} can be derived using the cosines law on the isosceles triangle AX_oA' in Figure 3-b, as presented in equation (6). Note that in the triangle, $\overline{X_oA} = \overline{X_oA'} = \vec{V}_i$, and $\overline{AA'} = r_{rvi}$. Hence,

$$r_{rvi} = \left|\vec{V}_i\right| \sqrt{2\left(1 - \cos(\omega_i \Delta t)\right)}. \tag{6}$$

Equation (7) presents the $\vec{V}_o$ inclusion criteria to the $\mathbf{VO}^+$. The inclusion into the **BV** zone in particular, can be derived by the subtraction of **VO** (equation (3)) from $\mathbf{VO}^+$.

$$\vec{V}_o \in \mathbf{VO}^+ \iff \left\{ \frac{\left[\vec{V}_o - \vec{A}_{vo^+}\right] \cdot \vec{D}_{vo}}{\left|\vec{V}_o - \vec{A}_{vo^+}\right| d_{vo}} > \cos \alpha_{vo^+} \quad \text{and} \quad d_{oi} < d_{avo} \right\} \tag{7}$$

For simplification, the plus (+) superscript, which indicates the addition of the **BV** set on the **VO**, is omitted in the remainder of this paper.

C. Avoidance Planes

Similar to the original VO-method, in order to avoid the obstacles, the ownship needs to update its velocity vector to a point outside every relevant **VO** set, into the set of the Avoidance Velocities, $\vec{V}_{avo}$. In the three-dimensional setup, these points of avoidance become more complex to determine, since there are more options in escaping either horizontally, vertically, or by a combination of the two. If the possible velocity updates can be represented with a particular three-dimensional curve or a sphere, then the options for avoidance are given by the intersection of that curve with the **VO** cone. The analytical derivation of such an intersection involves a complicated quartic equation, which defeats the purpose of the VO-method as a reactive and graphically understandable method for avoidance.

Therefore, the 3DVO method is accompanied by the concept of Avoidance Planes. This concept is used as a tool to logically and graphically describe the three-dimensional case into separate two-dimensional setups, and to find the appropriate velocity for avoidance. Therefore, instead of trying to derive all the possible resolutions for avoidance, the 3DVO method focuses only on a finite number of avoidance planes, which can be predefined based on the performance of the ownship. Ref 22 presents a similar method in which a three-dimensional case is broken down into two avoidance planes, which are the lateral plane (XY-Plane) and the longitudinal plane (XZ-Plane). The method presented in 27 also resembles the method with a very fine discretization of planes around the ownship X-axis.

The Avoidance Planes, P_ϕ, are defined as any plane in which the ownship velocity vector $\vec{V}_o$ lies, as shown in Figure 4-a. The avoidance is assumed to be conducted in one of these planes, which is parameterized by the angle of rotation of the plane, $\phi_{\mathbf{P}}$, around the vehicle X-axis. The **VO** set, therefore, is represented as a two-dimensional cross sectional area, $\mathbf{VO}_{\mathbf{P}_\phi}$. Since the **VO** is a right-cone, each $\mathbf{VO}_{\mathbf{P}_\phi}$s form a conic section, as shown in the example of four Avoidance Planes where $\phi_{\mathbf{P}} = -90^o, -45^o, 0^o$ and 45^o, in Figure 4-b. By comparing between the resulting $\mathbf{VO}_{\mathbf{P}_\phi}$, the ownship can choose the most fitting plane for an optimal avoidance. Section III presents an example of a strategy that includes an approach to choose between available avoidance planes.

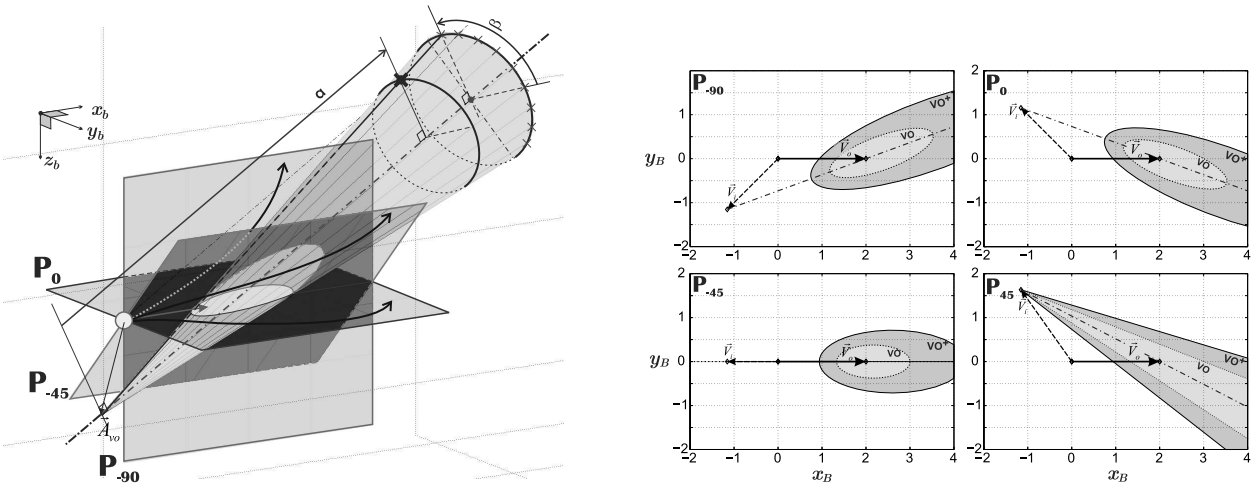

(a) (b)

Figure 4. The Avoidance Plane illustration intersecting the VO, (b) Conic-sections of the VO cone on several avoidance-planes.

The type of conic section can be determined by comparing the **VO**'s opening angle, α_{vo}, with the acute dihedral angle between the avoidance plane $\mathbf{P}_\phi$ and the cone effective base. This angle, denoted as $\delta_{\mathbf{P}_\phi}$, is derived in equation (8), i.e.,

$$\delta_{P_\phi} = \arccos\left(\frac{\vec{D}_{vo}}{d_{vo}}\begin{bmatrix}0\\ \sin\phi_{\mathbf{P}}\\ \cos\phi_{\mathbf{P}}\end{bmatrix}\right). \tag{8}$$

The conic section, therefore, is elliptical if $\delta_{\mathbf{P}_\phi} < \pi/2 - \alpha_{vo}$, and hyperbolic otherwise. Degenerate cases occur if additionally A_{vo} lies on the corresponding $\mathbf{P}_\phi$, which transforms the section into a single point, or

into a triangular section. Figure 4-b shows one example of this degenerate case in the $\mathbf{P_{45^\circ}}$, which results in a triangular section limited by the two intersecting lines of the $\mathbf{P_{45^\circ}}$ and the **VO** cone surface.

To derive the conic-section in an arbitrary avoidance plane, this paper expresses the **VO** cone parameters with respect to each avoidance plane ($\mathbf{P}_\phi$) reference using parametric equations, as presented in equations (9) through (14). Here, equation (9) is a standard cone parametric equation in Euclidean space rotated to align it with the $\vec{D}_{vo}$ vector, forming the Collision Cone **CC**. Adding the intended **VO** apex translates the cone into the Velocity Obstacle, as presented in equation (10). Finally, equation (11) rotates the previous **VO** with respect to each avoidance plane $\mathbf{P}_\phi$, into the $\{x_{vo}^\phi, y_{vo}^\phi, z_{vo}^\phi\}$ coordinates. Hence, the equations are

$$\begin{bmatrix} x_{cc} \\ y_{cc} \\ z_{cc} \end{bmatrix} = R_{\theta_{oi}|\psi_{oi}} \begin{bmatrix} a \\ a\tan\alpha_{vo}\cos\beta \\ a\tan\alpha_{vo}\sin\beta \end{bmatrix}, \tag{9}$$

$$\begin{bmatrix} x_{vo} \\ y_{vo} \\ z_{vo} \end{bmatrix} = \begin{bmatrix} x_{cc} \\ y_{cc} \\ z_{cc} \end{bmatrix} + \vec{A}_{vo}, \quad \text{and} \tag{10}$$

$$\begin{bmatrix} x_{vo}^\phi \\ y_{vo}^\phi \\ z_{vo}^\phi \end{bmatrix} = R_{p_\phi} \begin{bmatrix} x_{vo} \\ y_{vo} \\ z_{vo} \end{bmatrix}, \tag{11}$$

where

$$0 \le \beta < 2\pi, \qquad a \ge 0, \tag{12}$$

$$R_{\theta_{oi}|\psi_{oi}} = \begin{bmatrix} \cos\psi_{oi} & \sin\psi_{oi} & 0 \\ -\sin\psi_{oi} & \cos\psi_{oi} & 0 \\ 0 & 0 & 1 \end{bmatrix} \times \begin{bmatrix} \cos\theta_{oi} & 0 & -\sin\theta_{oi} \\ 0 & 1 & 0 \\ \sin\theta_{oi} & 0 & \cos\theta_{oi} \end{bmatrix}, \quad \text{and} \tag{13}$$

$$R_{P_\phi} = \begin{bmatrix} 1 & 0 & 0 \\ 0 & \cos\phi_{\mathbf{P}} & \sin\phi_{\mathbf{P}} \\ 0 & -\sin\phi_{\mathbf{P}} & \cos\phi_{\mathbf{P}} \end{bmatrix}. \tag{14}$$

The vertices in each avoidance-plane are derived by solving equation (11) for $z_{vo}^\phi = 0$, for every β. The resulting velocity obstacle conic section, denoted as $\mathbf{VO}_{\mathbf{P}_\phi}$, is therefore simplified into a polygon formed by a finite set of vertices, $\{x_{vo}, y_{vo}\}$ on the limiting curves. This method is chosen instead of other methods for deriving the $\mathbf{VO}_{\mathbf{P}_\phi}$ due to its simplicity and the required computational power, as compared to, for instance, the derivation of an exact quadric function. Moreover, it is also possible to use the parametric derivation of the $\mathbf{VO}_{\mathbf{P}_\phi}$ from a $\mathbf{S_{pz}}$ that is shaped other than a sphere, as long as the vertices that form the effective base of the **VO** cone (or pyramid) are determined.

The parameter β in equation (9) is the free-parameter of the **VO** effective circular base, whereas a is the free-parameter of the generating lines of the cone, which is bounded to be equal or greater than zero to remove vertices that lie on the other nappe of the cone. Both parameters are illustrated in Figure 4-a. For some cases of hyperbolic cross section, the bound of a can cause the omission of a significant part of the $\mathbf{VO}_{\mathbf{P}_\phi}$ section. Therefore, an additional extrapolation function is required in this case, so that the section can cover the reachable range of the $\vec{V}_o$.

The vertices that form the $\mathbf{VO}_{\mathbf{P}_\phi}$ section in each Avoidance Plane $\mathbf{P}_\phi$ are derived by solving the x_{vo}^ϕ and y_{vo}^ϕ in equation (11), for $z_{vo} = 0$. The following equation gives the value of a:

$$a\{z_{vo}^\phi = 0\} = \frac{A_{vo_z}\cos\phi_{\mathbf{P}} - A_{vo_y}\sin\phi_{\mathbf{P}}}{\begin{array}{l}(\sin\phi_{\mathbf{P}}\cos\theta_{oi} + \cos\phi_{\mathbf{P}})\sin\psi_{oi} \\ \quad + ((\cos\phi_{\mathbf{P}}\cos\theta_{oi} - \sin\phi_{\mathbf{P}}\sin\psi_{oi}\sin\theta_{oi})\sin\beta - \sin\phi_{\mathbf{P}}\cos\psi_{oi}\cos\beta)\tan\alpha_{vo}\end{array}} \tag{15}$$

The $\mathbf{VO}_{\mathbf{P}_\phi}$ for the degenerate cases can also be indicated using the numerator and denominator of equation (15). If the numerator is zero, all **VO** generating lines cross the avoidance plane on its apex. In

this case, the $\{x_{vo}, y_{vo}\}$ pair is determined by the values of β for which the denominator equal to zero. Zero, one, or two real value root(s) can be obtained as the solutions, by which, together with the cone apex, result in a single point, a straight line, or a triangular $\mathbf{VO}_{\mathbf{P}_\phi}$ section, respectively.

III. Strategy for Three-dimensional Avoidance

The proposed Three-dimensional Velocity Obstacle (3DVO) method are based on the three-dimensional sets and criteria described in the previous section. This section gives an example of a strategy using those definitions to generate a reactive avoidance maneuver in three dimensions. This strategy resembles the two-dimensional avoidance strategy in Ref.12, with an additional step to select the safe Avoidance Plane.

A. Avoidance Algorithm

The algorithm of avoidance is defined according to the condition of the ownship velocity vector $\vec{V}_o$ with respect to the defined sets in the 3DVO method. The algorithm is presented graphically in Figure 5, differentiated by the three modes of *mission*, *avoid*, and *maintain*.

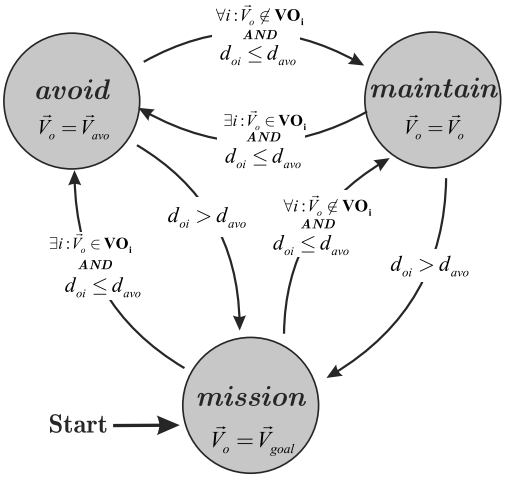

Figure 5. The Three-dimensional Velocity Obstacle method state diagram.

From a condition where the velocity vector is heading towards a designated goal, $\vec{V}_o = \vec{V}_{goal}$, whenever the $\vec{V}_o$ is included in the corresponding **VO**, or fulfilling equation (3), the ownship goes to the avoid mode. If the encounter is imminent ($d_{oi} \le d_{avo}$), but the $\vec{V}_o$ is not included in any of the **VO** set, the ownship can keep its heading towards its original goal in the maintain mode. In the avoiding mode, the $\vec{V}_o$ is updated continuously in the direction to the surface of **VO** until it steps outside the set, where the ownship is then switches to maintain mode. From maintain mode, the ownship might need to switch back to the avoid mode due to an obstacle maneuver, if the encounter is still imminent. Mission mode is restored whenever the encounters are no longer imminent, i.e., $d_{oi} > d_{avo}$.

In avoid mode, the ownship velocity vector is updated to a certain $\vec{V}_{avo}$ to get outside of the velocity obstacle set **VO**. The original VO-method commonly updates the ownship velocity to a point on the **VO** surface, denoted as the chosen escape point, $\vec{E}_{vo}$. This point can be chosen based on various strategies, such as by accelerating or decelerating while staying on the path, by turning without alteration of speed, or by simply choosing the closest point from the current velocity. This paper focuses on providing an escape route by pure turning with a certain rate of ω_{avo}, until the velocity vector aligns with the $\vec{E}_{vo}$. Hence, in a constant time-step Δt, the $\vec{V}_{avo}$ is defined in equation (16), where $\epsilon_{vo} = \arctan\left(\frac{E_{vo_y}}{E_{vo_x}}\right)$ is the angle of the vector $\vec{E}_{vo}$, in the chosen direction, from the ownship X-axis.

$$\vec{V}_{avo} = \begin{bmatrix} \cos\Theta & -\sin\Theta \\ \sin\Theta & \cos\Theta \end{bmatrix} \vec{V}_o, \qquad \text{where } \Theta = \arg\min\left\{\left|\omega_{avo}\Delta t\right|, \left|\epsilon_{vo}\right|\right\}. \tag{16}$$

By using the avoidance plane, the $\vec{E}_{vo}$ are determined in each plane as intersection points between the $\mathbf{VO}_{\mathbf{P}_\phi}$ and the circle of $\vec{V}_o$ rotation, as shown in Figure 6. These points are derived by solving the variables in equation (11) with $z_{vo} = 0$, where the $\{x^\phi_{vo}, y^\phi_{vo}\}$ satisfies equation (17), i.e.,

$$(x^\phi_{vo})^2 + (y^\phi_{vo})^2 = |\vec{V}_o|^2 \tag{17}$$

There will be a maximum of four solutions for the $\vec{E}_{vo}$ of the respective $\mathbf{VO}_{\mathbf{P}_\phi}$. The logical common choice from the four will be the one with the smallest ϵ_{vo} angle, which corresponds to the subtlest maneuver to avoid. No (zero) solution can result under two conditions: if either no part of the circle of $\vec{V}_o$ rotation is included in $\mathbf{VO}_{\mathbf{P}_\phi}$ or the whole circle is included. The latter condition happens when the ownship is too close to the obstacle, and should be prevented by conducting the avoidance maneuver well before the condition occurs.

An additional precaution is added in the algorithm when handling multiple encounters with eight obstacles, which is to only use $\vec{E}_{vo}$ points that are outside all other imminent $\mathbf{VO}_\phi$s. This is shown in Figure 6-b for a multiple-encounters situation, where only the two outermost points are valid $\vec{E}_{vo}$, from the total of six intersections of $\vec{V}_o$ with $\mathbf{VO}_\phi$.

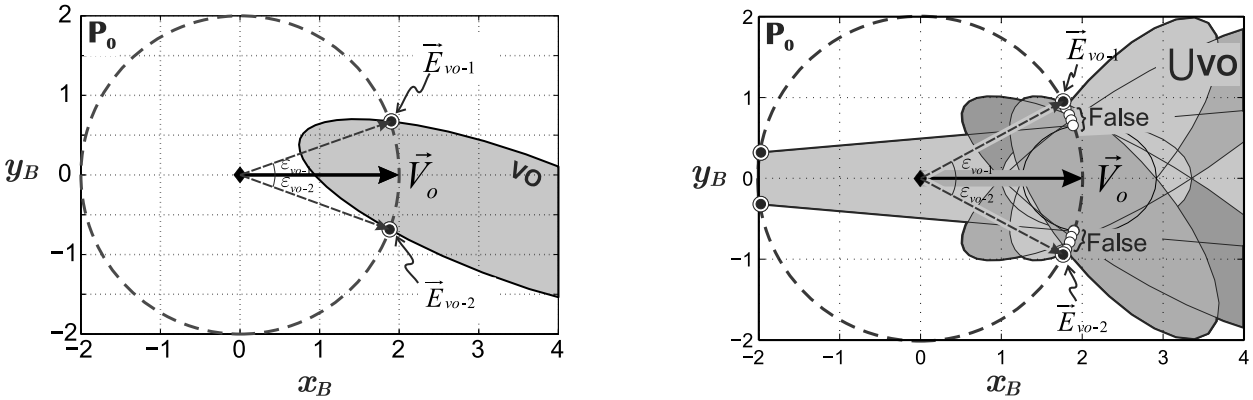

Figure 6. Avoidance by pure turning on $\mathbf{P_0}$ for cases with (a) one obstacle, (b) multiple obstacles

B. Choosing an Avoidance Plane

To demonstrate the 3DVO method performance, this paper uses an example with twelve Avoidance Planes, discretized evenly around the ownship X-axis, from $-\pi/2$ to $\pi/2$. The ownship therefore can choose the best avoidance plane by comparing the angle of rotation from the current velocity vector $\vec{V}_o$ to the $\vec{V}_{avo}$ point on the respective $\mathbf{VO}_\phi$ section. The avoidance plane, however, can provide other information to refine this strategy, especially when taking into account the obstacle maneuvers.

Besides using the angle of rotation, the best Avoidance Plane can be chosen by considering the shape of the $\mathbf{VO}_\phi$ section. A degenerate triangular shape, for example, is generally more dangerous than an ellipse or a circle, since it indicates that the corresponding Avoidance Plane might be the same plane the obstacle is moving in. Hence the avoidance maneuver can be nullified by an adverse movement of the obstacle. This danger can also happen in some case in avoidance on hyperbolic $\mathbf{VO}_\phi$ sections, due to the intersection of the $\mathbf{VO}_\phi$ with the $\mathbf{VO}$ cone effective base.

For those reasons, the Avoidance Plane is chosen by weighing the danger of each plane based on the shape of the $\mathbf{VO}_\phi$ section. Hyperbolic and triangular $\mathbf{VO}_\phi$ sections are dropped, while ellipsoidal sections are preferable, and therefore the avoidance is conducted in one of the $\mathbf{P}_\phi$ that has the particular shape. Afterwards the choice of $\mathbf{P}_\phi$ is based on which plane can provide a $\vec{E}_{vo}$ with the smallest rotation angle, ϵ_{vo}. Note that eccentricity of the $\mathbf{VO}_\phi$ section is not used as a deciding factor (which would result in a $\mathbf{P}_\phi$ that provides a $\mathbf{VO}_\phi$ section closest to that of a circle), since it does not necessarily correspond to the smallest ϵ_{vo}.

In case of multiple encounters, the avoidance plane is chosen from those that can give a minimum level of danger based on the inclusion of $\vec{V}_o$ and the shape of $\mathbf{VO}_\phi$, before deriving the one that has the smallest

angle of rotation to a possible $\vec{V}_{avo}$. Similarly to the single encounter case, avoidance-planes with triangular and hyperbolic $\mathbf{VO}_\phi$ are dropped. It is possible that a hyperbolic or triangular $\mathbf{VO}_\phi$ resulted in an avoidance plane, but does not include the $\vec{V}_o$. This particular plane is also dropped and considered more dangerous than those that have only ellipse sections.

C. Avoidance Turning Rate

Two parameters that need to be defined to apply the algorithm for 3DVO method are the avoidance distance d_{avo} and the avoidance turning rate ω_{avo}. The latter is required in an imminent encounter conflict where the vehicle dynamics cannot be neglected. The relationship between these two parameters can be viewed physically as the required maneuverability (ω_{avo}) for the available sensing capability (d_{avo}).

Consider an encounter between two vehicles, an ownship and an obstacle, initially positioned at $\vec{X}_o(0)$ and $\vec{X}_i(0)$, respectively, as shown in Figure 7. This type of conflict is considered as the worst avoidance scenario, when it must conduct the avoidance by turning to the opposite side of the obstacle $\mathbf{S_{pz}}$, or in this case, to the left. Turning to the right, on the other hand, would require the minimum effort since the vehicle is practically heading to the edge of the obstacle $\mathbf{S_{pz}}$. The radius required for turning to the left is therefore the smallest compared to any other colliding scenario, achievable with the largest value of avoidance turning rate, ω_{avo}.

From the initial point at $t = 0$, the ownship follows a circular path with radius $r_{avo} = |\vec{V}_o|/\omega_{avo}$, while the obstacle keeps its straight trajectory. The vehicles meet at $t = T$, where the ownship grazes the obstacle protected-zone, achieved by two conditions: the ownship position, $\vec{X}_o(T)$, is just at the edge of the $\mathbf{S_{pz}}$, and its vector of velocity $\vec{V}_o(T)$ is exactly tangential to that circle. This meeting condition is achieved when the value of the ownship avoidance turning rate, $\omega_{a.cr}$ is critical: if it is bigger, the avoidance path will have some offset from the $\mathbf{S_{pz}}$ edge and, if it is smaller, the ownship will penetrate the protected-zone. The critical value of ω_{avo} that is derived in this worst case scenario should be able to ensure safety in any other conflict scenario.

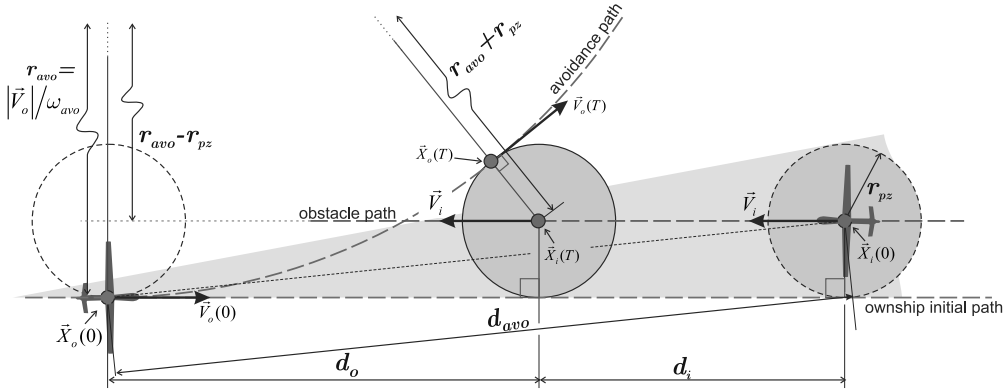

Figure 7. The worst scenario of conflict when the avoidance must be conducted by turning to the opposite direction

The relation between the critical value of the avoidance turning rate, $\omega_{a.cr}$, and the avoidance distance d_{avo}, can be derived by splitting it into two parts, the ownship part, d_o, and the obstacle part d_i. The former is derived using the critical conditions, which implies that the center of the circular avoidance path, the point of grazing, $\vec{X}_o(T)$, and the center of the $\mathbf{S_{pz}}$ lie on one straight line. A right triangle, therefore, can be formed with $r_{avo} + r_{pz}$ as the hypotenuse and $r_{avo} - r_{pz}$ and d_o as the legs. Hence d_o can be expressed as a function of the conflict geometry, as presented in equation (19). The d_{avo} is then solved as the hypotenuse of the triangle with d_o and the $\mathbf{S_{pz}}$ radius as the legs, as presented in equation (18).

The obstacle part of the avoidance distance, d_i, is a straight line that can be derived using the obstacle speed $|\vec{V}_i|$ and time, as expressed in (20). The time here has to match the time required by the ownship to reach point $\vec{X}_o(T)$ from its initial position. To derive the required time, the ownship $\vec{V}_o$ rotation can be used as follows: from the initial heading, $\psi_o(0) = 0$, the ownship rotates using a constant turning rate ω_{avo} until $\psi_o(T) = \omega_{avo}T$, which corresponds directly to the opposite angle of d_o, in the right triangle before. Equation (21) expresses the time in terms of the turning rate and the encounter geometry. Hence,

$$d_{avo} = \sqrt{(d_o + d_i)^2 + r_{pz}^2}, \tag{18}$$

$$d_o = \sqrt{(r_{avo} + r_{pz})^2 - (r_{avo} - r_{pz})^2} = 2\sqrt{\frac{|\vec{V}_o| r_{pz}}{\omega_{avo}}}, \tag{19}$$

$$d_i = |\vec{V}_i| T, \tag{20}$$

where

$$T = \frac{1}{\omega_{avo}} \arctan\left(\frac{d_o}{r_{avo} - r_{pz}}\right) = \frac{1}{\omega_{avo}} \arctan\left(\frac{d_o}{|\vec{V}_o|/\omega_{avo} - r_{pz}}\right). \tag{21}$$

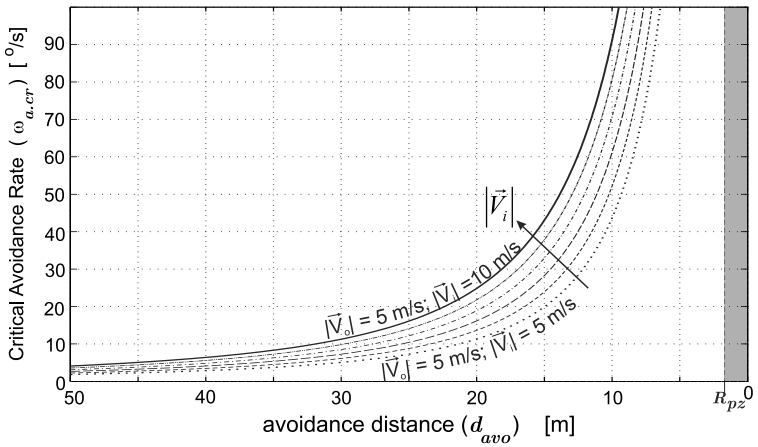

Figure 8. The curve of the critical avoidance turning rate, $\omega_{a.r}$, along the corresponding avoidance distance d_{avo}

Figure 8 shows the relation between the avoidance distance d_{avo} and the critical value of the avoidance turning rate $\omega_{a.cr}$, for the worst-case scenario explained before. The resulting curve is somewhat similar to the graph of the same parameter in Ref 12, which is obtained using a different method. The graph can also be viewed as a simplification of the Reachable Avoidance Velocity set (**RAV**),[13] or the command parameter space[18,23] employed in previous VO-method. In this case, the ownship need to choose an avoidance preference, i.e., by choosing a combination of d_{avo} and ω_{avo}, that is above the $\omega_{a.cr}$ curve.

Figure 8 is derived for a constant ownship speed, $|\vec{V}_o|$, of 5 m/s, facing head-on obstacles with speeds, $|\vec{V}_i|$, from 5 to 10 m/s. The required turning rate increases with obstacle speed, which suggest that to provide an adequate turning rate, the ownship needs to estimate first the speed of obstacle it might encounter during its operation. Furthermore, $\omega_{a.cr}$ increases exponentially with d_{avo} and practically sets a minimum distance of avoidance for a range of obstacle speeds. For instance, if it is estimated that the obstacle has speeds greater than 10 m/s, avoidance at 5 m from the obstacle by a pure turning would be impossible. These resulting $\omega_{a.cr}$ and the corresponding avoidance distances are used in the 3DVO method implementation, presented in the next section.

IV. Implementation

To evaluate its performance, the Three-dimensional Velocity Obstacle (3DVO) method and the proposed strategy are implemented in three different simulated cases. These cases are designed to test the method on generating three-dimensional resolutions, on handling maneuvering obstacles, and on handling multiple encounters. Each vehicle is modeled as a point-mass with designated initial velocity vector in the Euclidean space, moved in a constant time-step, $\Delta t = 0.1$ second. Note that to focus more on the method performance, these simulation does not include the dynamics of the vehicles, or the effect of the environment, e.g., wind and gravity.

Each vehicle independently generates conflict resolutions using the 3DVO method, based on their own detection of encounters in proximity. This detection includes the measurements for both ownship's and obstacles' states, which are listed together in Table 1, along with the assumptions used in the simulations. Every parameter is acquired seamlessly in every time-step, without delay or errors.

Table 1. Parameters required in the 3DVO method implementation

	Parameter	Notes and Assumptions	Unit
1	Ownship Position $\vec{X}_o$	Treated as the origin for all 3DVO implementation	[m]
2	Ownship Velocity $\vec{V}_o$	On ownship body axis, therefore only requires the initial speed, $\lvert\vec{V}_o\rvert$	[m/s]
3	Avoidance distance, d_{avo}	Avoidance distance preference for each vehicle is explicitly stated in each simulation setup	[m]
4	Avoidance turning rate, ω_{avo}	Avoiding turning rate is set at 10% above $\omega_{a.cr}$, corresponding to the preference of d_{avo}, as presented in Figure 7	[m/s]
5	Obstacle-i position, $\vec{X}_i$	Derived from the obstacle's angular position, i.e., the distance d_{oi}, azimuth ψ_{oi}, and elevation θ_{oi} angle, from the ownship axis	[-]
6	Obstacle-i velocity, $\vec{V}_i$	Obstacle-i absolute velocity, referred to the ownship axis	[m/s]
7	Obstacle-i possible turning rate, ω_i	For the derivation of the Buffer Velocity set **BV**. Assumed to be the same as the ω_{avo} of the ownship	[-/s]
8	Radius of protected-zone, r_{pz}	Every vehicle in the simulation assumes 1 meter as the radius of the protected-zone	[m]

The simulations are presented in a global frame of reference, such as shown in Figure 9, where each protected zone, $\mathbf{S_{pz}}$, is represented by a sphere with radius $r_{pz} = 1$ meter, and each velocity vector is visualized with a small cone. Note that the time slices in the frames are not ordered uniformly, instead, they are selected such that they show important phases of the simulation progression.

A. Two Vehicles Converging

Figure 9 shows the simulation of the case that has been used to explain the 3DVO method in previous sections, shown in Figure 2 to 3. This case serves as a proof of concept and the strategy of the 3D resolution generation using the avoidance planes. Two conflicting vehicles are involved, where the ownship is using the 3DVO method and conducts avoidance at d_{avo} of 10 meters and the obstacle stays on its initial flight path. Both vehicles move at 5 meters/second in a straight line, heading to a point far away from the initial position.

From the twelve avoidance planes provided by the 3DVO method's strategy, four avoidance-planes, i.e., $\mathbf{P_{-90^\circ}}$, $\mathbf{P_{-45^\circ}}$, $\mathbf{P_{0^\circ}}$, and $\mathbf{P_{45^\circ}}$, are shown. For each plane, both right and left turning are tested, making a total of eight resolution paths for the encounter case, as shown in a composite time-lapse frame in Figure 9. Every resolution successfully avoids the obstacle, as shown by the distance between the two vehicles in Figure 10-a. An offset from the obstacle r_{pz} results from the use of the buffer velocity set.

Figure 10-b shows the ownship drifting distance over time on each plane and each direction of avoidance. The figure shows almost the same maneuvering slope for every generated resolution. The vehicle's drift from its initial path can be evaluated by calculating the total path length of the drifting profile, Δl, as shown in the inset of the Figure 10-b. The value can be used to determine the efficiency of the avoidance maneuver. By comparison, turning to the right on $\mathbf{P_{45^\circ}}$ is the least efficient way to avoid for the encounter case. The more efficient way of avoidance is resulted by turning to the left on $\mathbf{P_{45^\circ}}$, $\mathbf{P_{0^\circ}}$ and $\mathbf{P_{-45^\circ}}$, or by turning to the right on $\mathbf{P_{-90^\circ}}$ and $\mathbf{P_{-45^\circ}}$, each differentiated by just a small margin. These results correspond to the $\mathbf{VO_{P_\phi}}$ section of each avoidance plane, shown in Figure 4-b, where the least efficient avoidance happens on the plane that has a triangular $\mathbf{VO_{P_\phi}}$ section, $\mathbf{P_{45^\circ}}$.

As a reactive avoidance method, the 3DVO is less computationally intensive compared to optimal control

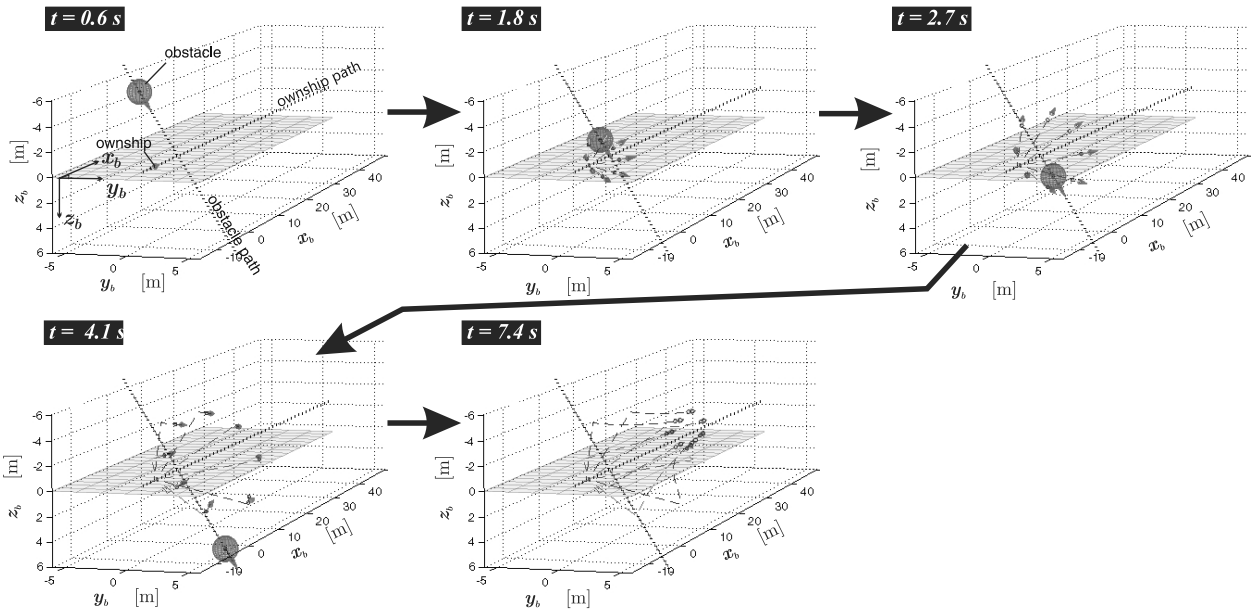

Figure 9. Simulation-1: The same case shown in Figure 2. Several choices of avoidance plane are given, $\mathbf{P}_{-90°}$, $\mathbf{P}_{-45°}$, $\mathbf{P}_{0°}$, and $\mathbf{P}_{45°}$

approaches, which require many iterations across control parameters for just one resolution. In contrast, compared to a simpler reactive method such as a basic PF-method that only requires one matrix summation from the obstacle relative position, the 3DVO is slower. However, the 3DVO process only starts when the criteria in equation (7) are fulfilled, while the PF-method starts whenever the vehicles are close enough, even for cases without possibility of collisions. This indicates that the 3DVO is more efficient in terms of the resulting avoidance path.

If an ownship only has a certain predefined avoidance plane to escape, e.g., always turn on its horizontal plane, then the only calculation is the criteria check in equation (7). The results are then used to determine the ownship states as depicted in Figure 5. On the other hand, when the ownship needs to decide which, among the available Avoidance Planes, is the best for the escape maneuver, the complexity of the 3DVO method increases. For this case, it requires four steps to determine a resolution, one of which consist of a series of matrix manipulations (one summation and two multiplications). This step depends directly on the number of vertices involved when determining the $\mathbf{VO}_{\mathbf{P}_\phi}$, and on the number of available Avoidance Planes. The simulations in this research use at most 36 vertices and twelve Avoidance Planes, for which the number of calculations is still far less than the number of iterations across parameters in an optimal control scheme for avoidance, such as dynamic programming.[5]

B. Multiple Heterogeneous Conflicts

This simulation tests the overall capability of the 3DVO method: generating resolutions in a multiple and dynamic encounter situation. Here, eight vehicles are tested in a cube-like setup, as shown in Figure 11. Each sphere in the figure represents half the radius of the protected-zone to conserve the visualization of the collision, such that vehicle collisions are shown by two touching spheres, instead of two coincident spheres. This setup is a three-dimensional extension of the eight-vehicle super-conflict case used in previous studies,[12,28,29] which tested the two-dimensional collision-avoidance method.

The vehicles in this simulation are heterogeneous, meaning that each of them has a different speed, $|\vec{V}|$, and a different preference of where to start the avoidance, d_{avo}. The speed of each of the vehicles is uniformly randomized within a range of 5 – 10 meters/second. Furthermore, the d_{avo} is uniformly randomized as well, within 10 - 15 meters, with avoidance turning-rate, ω_{avo} that is 10% higher than the critical turning rate shown in Figure 8. The initial positions in the cube are selected along the respecting space diagonals, to make all vehicles reach the center of the cube at the same time.

The 3DVO method and strategy are used in each vehicle, which enable it to avoid others by turning

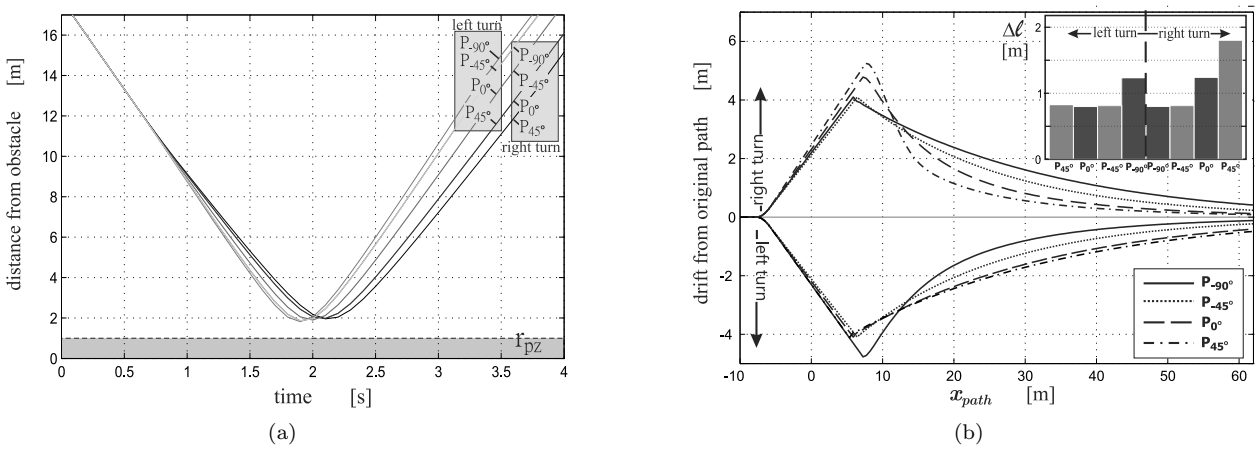

Figure 10. Simulation-1: (a) Distance between vehicles and (b) ownship drifting from original path

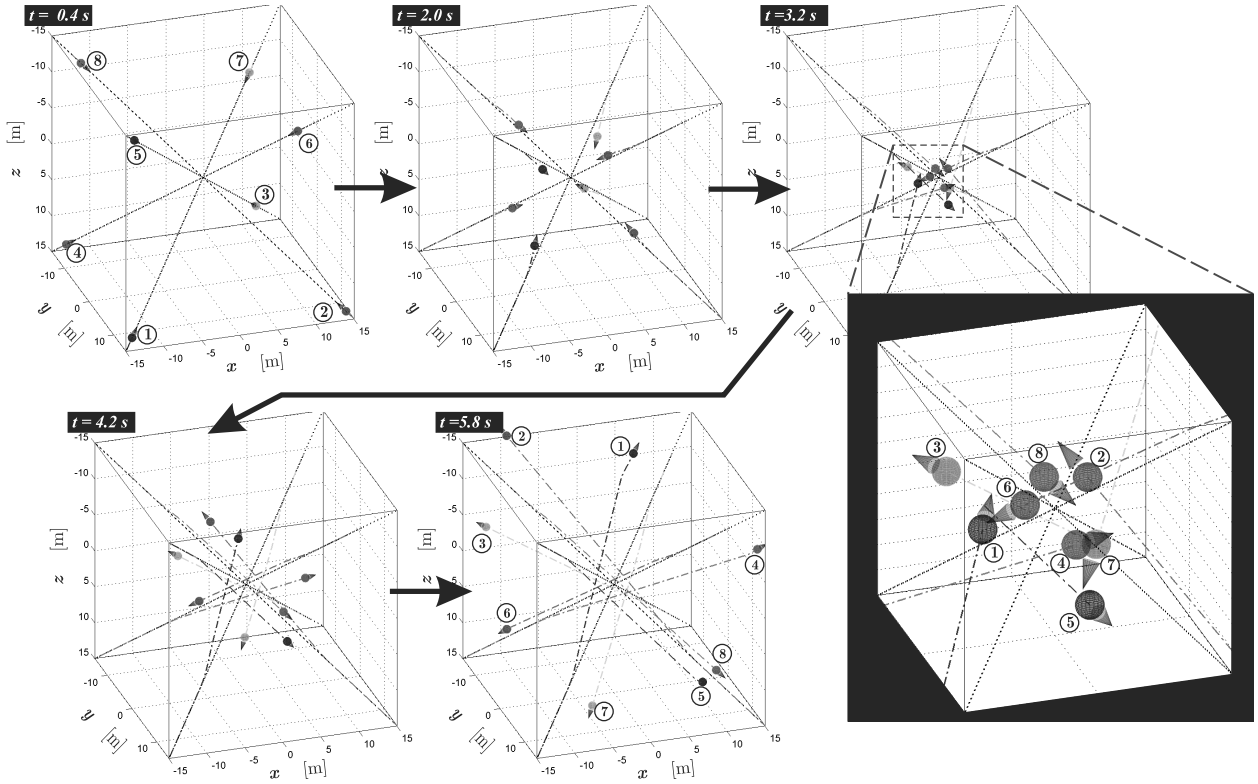

Figure 11. Simulation-2: Multiple 3-dimensional conflicts, in randomly heterogeneous setup.

on one of the twelve possible avoidance-planes. With all vehicles avoiding in a random and uncoordinated manner, the situation becomes dynamic: each vehicle is facing obstacles that can change direction at an arbitrary time. Figure 11 shows one example result of the random scenario.

The simulation shows that the heterogeneous setup produces a variation of resolution maneuvers, which ultimately resolves the conflict independently for every vehicle. The work of the 3DVO method can be represented by the change of the flight path and the heading angle, as shown in Figure 12. Here, each vehicle has a different preference of avoidance, with vehicle 3 and 5 having the biggest change of direction. The dynamic situations are shown by the modes of the vehicles, where the avoidance mode occurs more than once for some of the vehicles. The change of direction between the avoidance modes also demonstrates the

variation of the avoidance-plane chosen during the maneuver, exploiting the three-dimensional space.

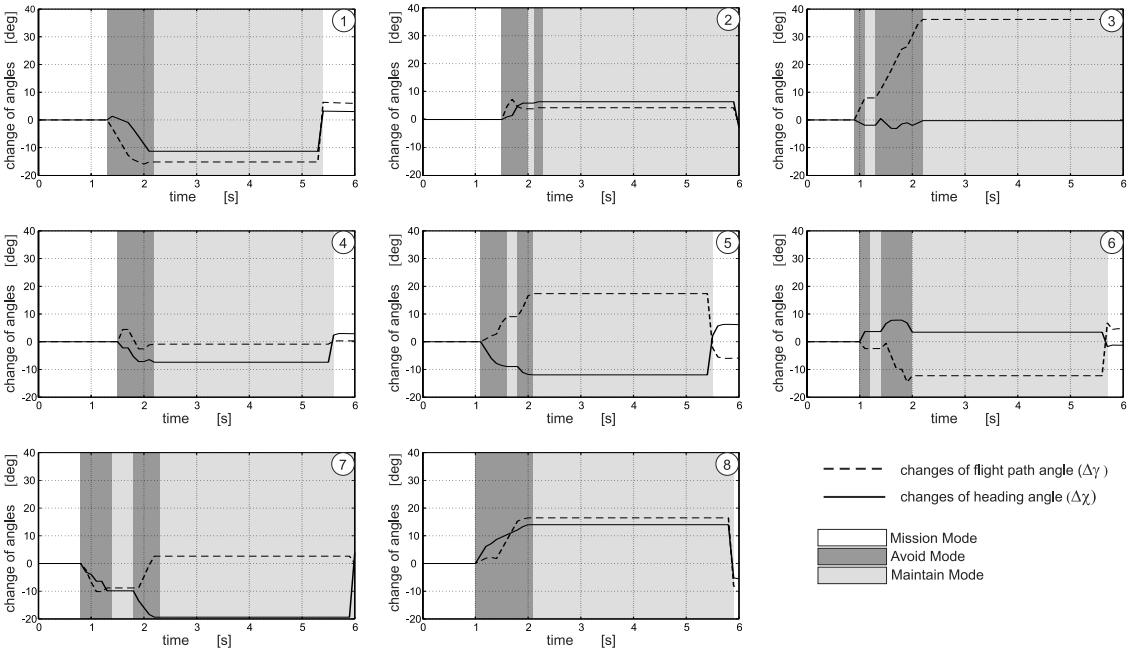

Figure 12. Simulation-2: Changes of vehicles directional angle and the modes of the 3DVO method, during avoidance

C. 3DVO method Validation

This third implementation is used to validate the performance of the 3DVO method in generating three-dimensional resolutions for various three-dimensional conflicts by using Monte Carlo simulations. The eight-vehicle super-conflict scenario in the previous subsection is used again with an additional random factor for the vehicle position. As shown in an example in Figure 13, besides the vehicle speeds and the avoidance distances, the unit vector of the positions, $\hat{x}$, $\hat{y}$, and $\hat{z}$, are also uniformly randomized, while keeping each octant of the Euclidean space having one representative vehicle. The space-diagonal paths for each vehicles, therefore, vary in orientation and thus results in more stressful scenarios than those in the previous subsection. The initial positions are then adjusted to force all vehicles to reach the origin at the same time. Moreover, an exception is added to drop any generated scenario that starts with two vehicles or more that are already in an imminent encounter, or in a collision.

For a limited time frame, the expected value of collision probability and its variance are calculated using equations (22) and (23). Along with the complete 3DVO method simulation, five other variations of the method are also tested for comparison, as listed in Table 2. The last row of the table presents the results of the PF-method implementation to the super-conflict setup, in order to have have an exact comparison of the 3DVO with other reactive methods. It should be noted, however, that the PF-method[6] implemented is only in its most basic form with a 3D realization, i.e., adding a negative gain to the ownship velocity vector based on the relative position of each imminent obstacle.

A total of 25,000 different initial condition samples, N_{MC}, are considered. The number is selected by observing the convergence of the expected value of P_{col} results for each series of the simulations. A collision is marked when at least two vehicles have a distance less than the designated radius $r_{pz} = 1$ meter, where the simulation is stopped and added to the collision occurrence, N_{col}. Any collision that may occur afterwards is neglected. Equation (24) gives the precision of the Monte Carlo runs with a 99.95% confidence interval. Note that the result does not follow one vehicle in particular, but rather the general probability in the airspace sample. The equations to derived the Monte Carlo parameters are

$$E\left[P_{col}\right] = \frac{1}{N_{MC}} \sum_{i=1}^{N_{MC}} n_{col_i}, \tag{22}$$

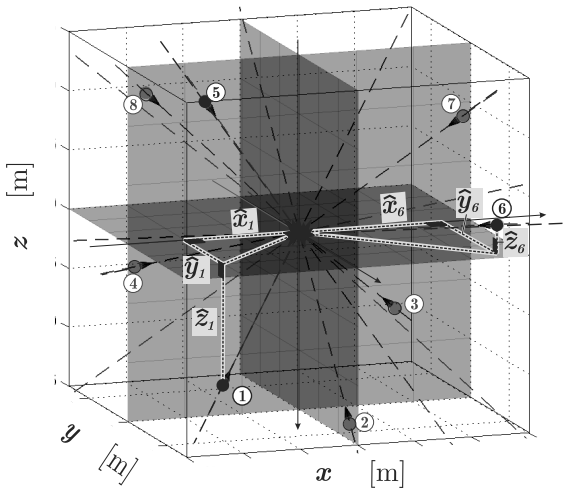

Figure 13. Simulation-3: Initial parameter randomization setup for the super-conflict scenarios

$$\sigma_{col}^2 = \frac{1}{N_{MC}} \sum_{i=1}^{N_{MC}} \left(n_{col_i} - E\left[P_{col}\right]\right)^2, \qquad \text{and,} \tag{23}$$

$$P_{col} = E\left[P_{col}\right] \pm \frac{3.3\sigma_{col}}{\sqrt{N_{MC}}}. \tag{24}$$

The result of the Collision Frequency is presented in Table 2. It is shown that two-dimensional avoidance is not enough to solve a three-dimensional uncoordinated conflict. The use of multiple avoidance planes, which exploits the three-dimensional space more, gives a lower collision occurrences even without considering the obstacle maneuver. However, it is shown that the use of the Buffer Velocity for the collision reduction is more effective than the addition of Avoidance Planes. Ultimately, the 3DVO method and the proposed strategy resulted in zero collision occurrence for the 25,000 samples of random three-dimensional, uncoordinated, dynamic multiple conflicts. The probability of collisions, however, cannot be determined within the tested samples due to the insufficient variation of results.

Table 2. Comparison of collision occurrences in various method, for the 25,000 random samples

Methods	Predefined Avoidance Plane	**BV** Application	Collision Occurrence	Collision Probability	note
1	XY-plane	NO	1428	5.75 ± 0.48 %	VO-method
2	XY-plane	YES	260	1.04 ± 0.21 %	
3	XY & YZ -plane	NO	386	1.52 ± 0.26 %	
4	XY & YZ -plane	YES	23	0.09 ± 0.06 %	
5	12 plane (distributed)	NO	256	1.02 ± 0.21%	
6	12 plane (distributed)	YES	0	na	3DVO
7	-	-	4521	18.03 ± 0.80 %	PF-method

The basic PF-method result is evidently inferior, even if it is compared with the two-dimensional VO-method. This, however, is expected since the PF-method is not designed either for multiple encounters, or for dynamic maneuvering obstacles.

V. Conclusions

This paper described a novel conflict resolution method called the Three-Dimensional Velocity Obstacle (3DVO) method. The method is designed to generate a reactive three-dimensional avoidance maneuver for an Unmanned Aerial Vehicle (UAV) to resolve three-dimensional conflicts. The method takes into account uncoordinated obstacle movement, as well as multiple obstacle encounters. The overall 3DVO method performance has been demonstrated using a series of simulations, which resulted in zero collisions for all given conflict scenarios.

The performance of the 3DVO method is the result of three key features: the addition of the Buffer Velocity zone, the concept of the Avoidance Planes, and the derivation of the required avoidance turning-rate. The Buffer Velocity zones ensures safety of the UAV when facing obstacles with adverse movement during the avoidance process. The Avoidance Planes enables the three-dimensional exploitation that reduces the frequency of collision. These planes can be linked directly to the maneuverability of the UAV. Lastly, the required avoidance turning rate derivations give a quantitative relationship between the UAV maneuverability (turning-rate) and available sensing capability (avoidance distance). This relationship can be used to determine a safety measure in UAV design.

While the 3DVO method shows many promising results, there is still room for improvement. The method has yet to be tested in higher-density super-conflict cases. The influence of uncertainty has yet to be considered, which is necessary for conflict scenarios that assume the use of on-board sensors. Real-life flight testing is also required before the 3DVO can be considered ready to be implemented in a UAV. Nevertheless, the 3DVO method has been demonstrated and performed as intended to aid UAV's Conflict Detection and Resolution system, towards its integration into the airspace system.

References

[1]Dalamagkidis, K., Valavanis, K. P., and Piegl, L. A., "On integrating unmanned aircraft systems into the national airspace system," *International Series on Intelligent Systems, Control, and Automation: Science and Engineering*, Vol. 36, Springer Science+Business Media, 1st ed., 2009, doi:10.1007/978-94-007-2479-2.

[2]Jenie, Y. I., Kampen, E.-J. V., Ellerbroek, J., and Hoekstra, J. M., "Conflict detection and resolution system architecture for unmanned aerial vehicles in civil airspace," *AIAA Infotech @ Aerospace*, AIAA, Kissimmee, FL, 2015, AIAA 2015-0483, doi:10.2514/6.2015-0483.

[3]Nikolos, I., Valavanis, K., Tsourveloudis, N., and Kostaras, A., "Evolutionary algorithm based offline/online path planner for UAV navigation," *IEEE Transactions on Systems, Man, and Cybernetics, Part B: Cybernetics*, Vol. 33, No. 6, 2003, pp. 898–912, doi: 10.1109/TSMCB.2002.804370.

[4]Borrelli, F., Subramanian, D., Raghunathan, A., and Biegler, L., "MILP and NLP techniques for centralized trajectory planning of multiple unmanned air vehicles," *Proceedings of the American Control Conference*, Vol. 2006, 2006, pp. 5763–5768, doi: 10.1109/ACC.2006.1657644.

[5]Kochenderfer, M. J., Holland, J. E., and Chryssanthacopoulos, J. P., "Next generation airborne collision avoidance system," *Lincoln Laboratory Journal*, Vol. 19, No. 1, 2012, pp. 55–71, doi: 10.2747/1548-1603.48.1.24.

[6]Khatib, O., "Real-Time obstacle avoidance for manipulators and mobile robots," *The International Journal of Robotics Research*, Vol. 5, No. 1, 1986, pp. 90–98, doi:10.1177/027836498600500106.

[7]Prandini, M., Hu, J., Lygeros, J., and Sastry, S., "A probabilistic approach to aircraft conflict detection," *IEEE Transactions on Intelligent Transportation Systems*, Vol. 1, No. 4, Dec 2000, pp. 199–220, doi:10.1109/6979.898224.

[8]Coso, F. A. and Castaeda, M. P., "Autonomous robot navigation using adaptive potential fields," *Mathematical and Computer Modelling*, Vol. 40, No. 910, 2004, pp. 1141 – 1156, doi: 10.1016/j.mcm.2004.05.001.

[9]Lam, T., Boschloo, H., Mulder, M., and Van Paassen, M., "Artificial force field for haptic feedback in UAV teleoperation," *Systems, Man and Cybernetics, Part A: Systems and Humans, IEEE Transactions on*, Vol. 39, No. 6, Nov 2009, pp. 1316–1330, doi:10.1109/TSMCA.2009.2028239.

[10]Chakravarthy, A. and Ghose, D., "Obstacle avoidance in a dynamic environment: a collision cone approach," *Systems, Man and Cybernetics, Part A: Systems and Humans, IEEE Transactions on*, Vol. 28, No. 5, Sep 1998, pp. 562–574, doi:10.1109/3468.709600.

[11]Chakravarthy, A. and Ghose, D., "Generalization of the collision cone approach for motion safety in 3-D environments," *Autonomous Robots*, Vol. 32, No. 3, 2012, pp. 243–266, doi:10.1007/s10514-011-9270-z.

[12]Jenie, Y. I., Kampen, E.-J. v., de Visser, C. C., Ellerbroek, J., and Hoekstra, J. M., "Selective velocity obstacle method for deconflicting maneuvers applied to unmanned aerial vehicles," *Journal of Guidance, Control, and Dynamics*, Vol. 38, No. 6, 2015, pp. 1140–1146, doi: 10.2514/1.G000737.

[13]Fiorini, P. and Shiller, Z., "Motion planning in dynamic environments using velocity obstacles," *The International Journal of Robotics Research*, Vol. 17, No. 7, 1998, pp. 760–772, doi:10.1177/027836499801700706.

[14]Kluge, B. and Prassler, E., "Recursive probabilistic velocity obstacles for reflective navigation," *Field and Service Robotics*, edited by S. Yuta, H. Asama, E. Prassler, T. Tsubouchi, and S. Thrun, Vol. 24 of *Springer Tracts in Advanced Robotics*, Springer Berlin Heidelberg, 2006, pp. 71–79, doi:10.1007/10991459_8.

[15]van der Berg, J., Lin, M., and Manocha, D., "Reciprocal velocity obstacles for real-time multi-agent navigation," *International Conference on Robotics and Automation*, IEEE, Pasadena, CA, USA, 2008, doi:10.1109/ROBOT.2008.4543489.

[16]van Dam, S. B. J., Mulder, M., and Van Paassen, M., "Ecological interface design of a tactical airborne separation assistance tool," *Systems, Man and Cybernetics, Part A: Systems and Humans, IEEE Transactions on*, Vol. 38, No. 6, Nov 2008, pp. 1221–1233, doi:10.1109/TSMCA.2008.2001069.

[17]Heylen, F. M., van, S. B. J., Mulder, M., and van Paassen, M. M., "Design and evaluation of a vertical separation assistance display," *AIAA Guidance, Navigation, and Control Conference and Exhibit*, Honolulu (HI), 2008, AIAA 2008-6969, doi:10.2514/6.2008-6969.

[18]Wilkie, D., van den Berg, J., and Manocha, D., "Generalized velocity obstacles," *Intelligent Robots and Systems, 2009. IROS 2009. IEEE/RSJ International Conference on*, Oct 2009, pp. 5573–5578, doi:10.1109/IROS.2009.5354175.

[19]Snape, J., van den Berg, J., Guy, S., and Manocha, D., "The hybrid reciprocal velocity obstacle," *Robotics, IEEE Transactions on*, Vol. 27, No. 4, Aug 2011, pp. 696–706, doi:10.1109/TRO.2011.2120810.

[20]Ellerbroek, J., Visser, M., van Dam, S. B. J., Mulder, M., and van Paassen, M. M., "Design of an airborne three-dimensional separation assistance display," *IEEE Transactions on Systems, Man, and Cybernetics, part A: Systems and Humans*, Vol. 41, No. 6, 2011, pp. 863–875, doi:10.1109/TSMCA.2010.2093890.

[21]Ellerbroek, J., Mulder, M., and van Paassen, M. M., "Evaluation of a separation assistance display in a multi-actor experiment," *Proceedings of the 16th International Symposium on Aviation Psychology*, 2011.

[22]Ellerbroek, J., Brantegem, K. C. R., van Paassen, M. M., and Mulder, M., "Design of a co-Planar airborne separation display," *IEEE Transactions on Human-Machine Systems*, Vol. 43, No. 3, 2013, pp. 277–289, doi:10.1109/TSMC.2013.2242888.

[23]Peterson, C. and Barton, J., "Virtual structure formations of cooperating UAVs using wind-compensation command generation and generalized velocity obstacles," *Aerospace Conference, 2015 IEEE*, March 2015, pp. 1–7, doi:10.1109/AERO.2015.7118926.

[24]Luongo, S., Corraro, F., Ciniglio, U., Di Vito, V., and Moccia, A., "A novel 3D analytical algorithm for autonomous collision avoidance considering cylindrical safety bubble," *Aerospace Conference, 2010 IEEE*, March 2010, pp. 1–13, doi:10.1109/AERO.2010.5446780.

[25]Jenie, Y. I., Kampen, E.-J. V., de Visser, C. C., Ellerbroek, J., and Hoekstra, J. M., "Three-dimensional velocity obstacle method for UAV deconflicting maneuvers," *AIAA Guidance, Navigation, and Control Conference*, AIAA, Kissimmee, FL, 2015, AIAA 2015-0592, doi:10.2514/6.2015-0592.

[26]Chakravarthy, A. and Ghose, D., "Collision cones for quadric surfaces," *Robotics, IEEE Transactions on*, Vol. 27, No. 6, Dec 2011, pp. 1159–1166, doi:10.1109/TRO.2011.2159413.

[27]Hurley, R. D., Lind, R., and Kehoe, J. J., "A torus based three dimensional motion planning model for very maneuverable micro air vehicles," *AIAA Guidance, Navigation, and Control Conference 2013*, AIAA, Boston, MA, 2013, AIAA 2013-4938, doi:10.2514/6.2013-4938.

[28]Hoekstra, J. M., Ruigrok, R., and van Gent, R., "Free flight in a crowded airspace?" *Air Transportation Systems Engineering, Progress in Astronautics and Aeronautics*, edited by P. Zarchan, A. G. Zellweger, and G. L. Donohue, Vol. 193, American Institute of Aeronautics and Astronautics, 2001, pp. 533–545, doi:10.2514/5.9781600866630.0533.0545.

[29]Hoekstra, J., van Gent, R., and Ruigrok, R., "Designing for safety: the free flight air traffic management concept," *Reliability Engineering & System Safety*, Vol. 75, No. 2, 2002, pp. 215 – 232, doi:10.1016/S0951-8320(01)00096-5.